J. Fluid Mech. (1971), *vol.* 50, *part* 3, *pp.* 469–480
Printed in Great Britain

The determination of the interfacial tension between two liquids

By JEROME H. MILGRAM AND ROBERT G. BRADLEY†
Massachusetts Institute of Technology

(Received 21 January 1971 and in revised form 28 June 1971)

The problems commonly encountered in the measurement of the interfacial tension between two liquids by capillary tube or force measurement are described. In order to avoid such problems, a new method of measurement of the interfacial tension is developed here which is based on the details of axisymmetric capillary waves which can be generated on the interface. Analyses relating these details to the interfacial tension and showing how the details can be measured photographically are given. An apparatus for making these photographic measurements is described and photographs made with such an apparatus are presented. An analysis of these photographs is given which gives the interfacial tensions for the interfaces shown.

1. Introduction

The usual methods of determining the surface tension on a liquid–gas interface are by measurement of the rise of the liquid in a capillary tube or by measurement of the force necessary to pull an object, having a known length of edge in contact with the interface, off the interface. Success of the capillary tube method requires that the contact angle of the liquid on glass in the gaseous environment be nearly zero. For many liquid–gas combinations this condition is satisfied and accurate determination of the surface tension can be obtained if the glass is extremely clean. Devices which measure the force necessary to pull an object off the interface typically use a ring of circular cross-section lying horizontally on the surface, or a vertical plate with one edge in contact with the surface, as the object. If care is taken so that the pulling force is evenly distributed over the edge of the object in contact with the fluid surface, an accurate determination of the surface tension can be made.

When the interfacial tension of a liquid–liquid interface is to be determined, the problem is much more difficult. Frequently, the capillary rise is into an opaque liquid so that it cannot be observed for visual measurement. This problem confronted Bartell & Miller (1928), who were attempting to measure the tension on the interface between crude oil and water. They constructed an apparatus that allowed visual measurement of the capillary rise of the interface. Figure 1 shows their apparatus with the figure caption containing a short excerpt from their description of its use.

Recent studies of oil pollution have resulted in renewed interest in determining

† Present address: Sandia Corporation.

the interfacial tension between various oils and water. The reason for this is that when an oil slick is thin, its spreading rate is affected by the interfacial tensions on the three interfaces between the oil, water and air as shown by Fay (1969). The two liquid–air surface tensions can easily be measured by the methods described above, but determination of the oil–water interfacial tension is less straightforward.

We have carried out experiments with apparatus of Bartell & Miller as well as with an apparatus which operates on the same principle but is easier to use (figure 2). The results of repeated experiments with any given apparatus and the

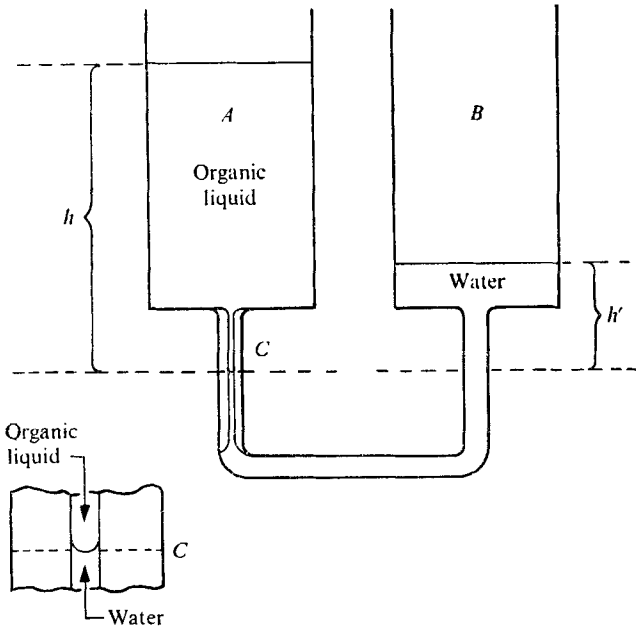

FIGURE 1. The apparatus of Bartell & Miller, and their description of its use. "In case the organic liquid to be used is less dense than water, the latter (about 10 cc or more) is put into cup *B*. It will completely fill the glass tube and will mount to the top of the capillary tube. Immediately, the organic liquid is introduced at *A* so that a liquid–liquid interface is formed at the upper end of the capillary. More liquid is added, finally drop by drop until the interfacial meniscus is forced down even with the calibration mark at *C*. Readings *h* and *h'*, the heights of the organic liquid and water, respectively, above this meniscus, are now taken by means of a cathetometer." (Excerpt from Bartell & Miller (1929).)

same sources of oil and water were inconsistent with each other. One of the reasons for this appears to be that the contact angle of the interface with the glass tubes was not fixed. In fact, in some instances it appeared that the oil wetted the glass more than did the water, and in other instances the opposite case was true.

One of the major difficulties in determining liquid–liquid interfacial tensions by the ring or plate method is the selective wetting of the edge, sometimes by one of the fluids and sometimes by the other. Further problems occur when the interfacial tension is very low. When certain contaminants are present, oil–water interfacial tensions less than one dyne per centimetre have been reported. When the interfacial tension is this low it is difficult to obtain a small fractional

error in the measurement. The error is increased by mechanical vibrations in the apparatus, which usually come from external sources, resulting in premature parting of the object from the interface.

Because of the difficulties encountered in determining liquid–liquid interfacial tensions by traditional methods, we have devized a method of determining these tensions from the details of capillary waves on the interfaces. Initially, attempts were made to generate two-dimensional capillary waves of known frequency on an interface in a channel by means of an oscillating wall. Reliable generation of such waves on an oil–water interface was found to be impossible owing to emulsification of the oil and water by the wavemaker and other three-dimensionless effects.

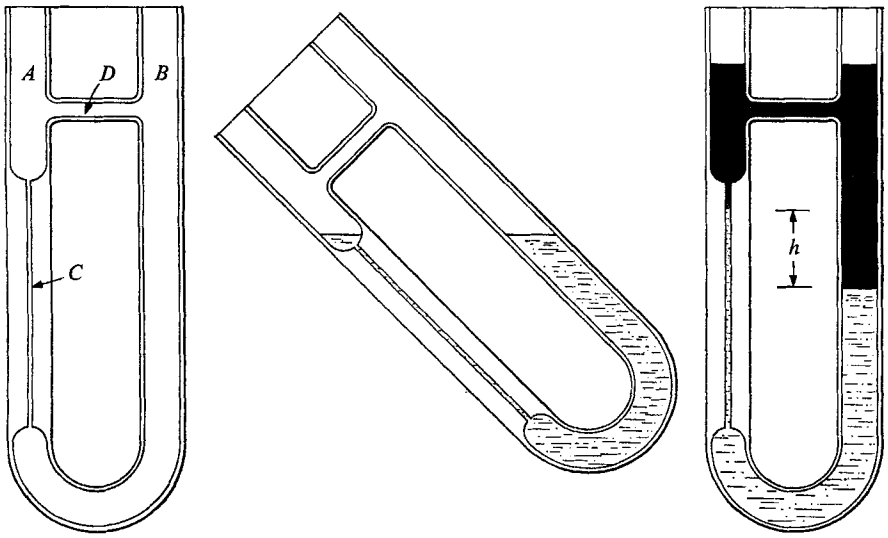

FIGURE 2. The apparatus consists of a U tube, one leg containing the capillary tube C. The two legs are joined near their tops by the connecting tube D. To use the apparatus, it is rotated to the left, and the more dense fluid is slowly introduced into tube A until the capillary tube is completely filled as shown in (b). Then the less dense fluid is slowly added to either A or B or both as the apparatus is rotated into a vertical position. This is continued until the less dense fluid completely fills the connecting tube D as shown in (c). The difference in height h between the two interfaces is then measured, and $T = \frac{1}{2}rhg(\rho_+ - \rho_-)$ if the more dense fluid completely wets the apparatus at the interface. T = surface tension, r = capillary tube radius, g = acceleration due to gravity, ρ_+ = density of heavier fluid, ρ_- = density of lighter fluid.

More success was obtained with axisymmetric waves in a cylindrical container. These waves were generated by a rod positioned along the axis of the container with one end near the interface and which was vibrating axially at a fixed frequency. The interfacial tension was then obtained from calculations based on photographic records of the waves.

2. Theory

The first problem considered here is the determination of the form of infinitesimal axisymmetric waves generated at the centre of the interface between

two fluids in a cylindrical container as shown in figure 3. When one of the fluids is translucent, points of zero wave height on the interface can be estimated by optical methods subsequently described. Therefore, a means of finding the interfacial tension from a knowledge of the positions of zero wave height is needed.

When small waves are generated on an interface between two fluids by small axial sinusoidal oscillations of a rod of radius R_0, having one end near the centre of the interface (figure 3); the waves propagate radially outwards and, in the absence of viscosity, attenuate in height such that their mean energy flux is constant as their circumference is increased. Such waves would be reflected from the side wall of the container and their height would increase as they propagated radially inwards with the resulting combination of ingoing and outgoing waves forming a standing wave. When one or both of the fluids have a small amount of

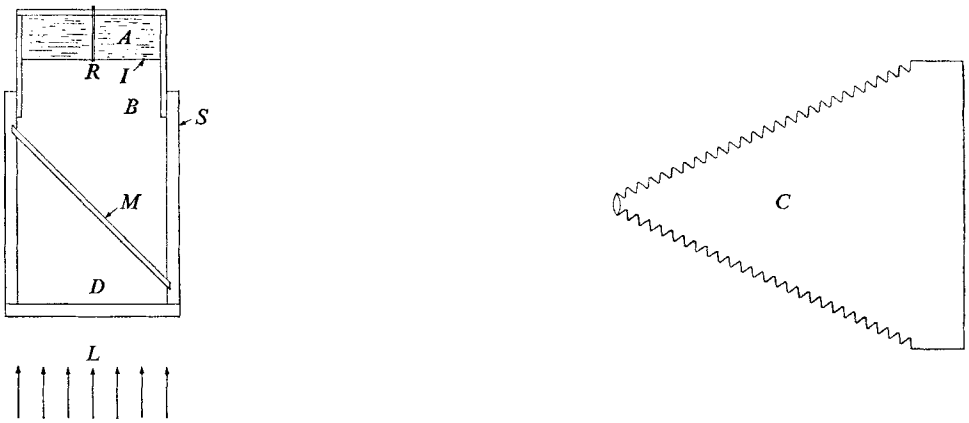

FIGURE 3. The apparatus for the generation and photography of axisymmetric waves on an interface. A, lighter fluid; B, D, heavier fluid; C, camera; I, interface; L, incident beam of parallel light; M, half silvered mirror; R, rod of radius R_0 whose end generates axisymmetric interfacial waves when oscillated in axial direction; S, container whose upper part is axisymmetric with radius R_1. The lower part need not be axisymmetric because the wave motion decreases very rapidly with increasing distance from the interface.

viscosity, the principal viscous effect on the interfacial waves is a viscous attenuation of their amplitude as they propagate. If the viscous attenuation of a wave is small during the time it takes the wave to travel a wavelength, the fluid motion is nearly equal to that which would exist in the absence of viscosity, except for the small viscous attenuation and thin boundary layers near the interface. If the distance over which there is a large viscous attenuation is small compared to the radius of the vessel R_1 the amplitude of the waves incident on the side wall will be negligible as will be the amplitude of the reflected wave.

The conditions of small viscous attenuation over a wavelength and large viscous attenuation over a distance equal to the radius of the container are frequently met. For this reason, the following analysis will be carried out for a container of infinite radius. The wavelengths of the interfacial waves to be considered are small compared to the depth of either fluid so the depths will be taken as infinite in the analysis.

The idealized geometry used for this analysis is shown in figure 4. Since infinitesimal waves are being considered linearized water-wave theory will be used, which together with the sinusoidal motions in time of the wave generating rod, requires that the entire problem have a sinusoidal time dependence. Therefore, equations will be written in terms of the complex amplitudes of physical quantities. At any point in the sequel, any physical quantity may be formed by multiplying its complex amplitude $e^{i\omega t}$ and subsequently taking the real part. Physical quantities are denoted by lower case characters and their complex amplitudes are denoted by corresponding upper case characters.

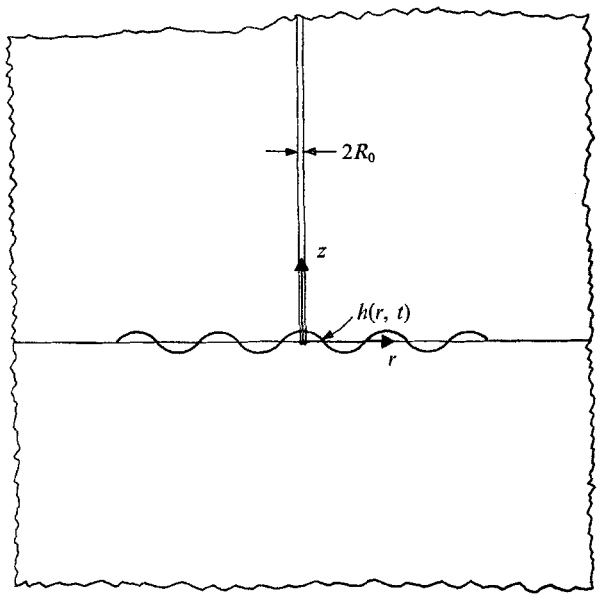

FIGURE 4. Idealized geometry for the wave analysis. $h(r, t)$ is the interfacial wave elevation.

The fluids are considered to be incompressible so velocity potentials Φ^+ and Φ^- can be defined in the upper and lower fluids respectively such that

$$\mathbf{V}^{\pm} = \nabla\Phi^{\pm}, \tag{1}$$

where V is the complex amplitude of the fluid velocity. Since viscosity is to be neglected, the complex amplitudes of the velocity potentials satisfy Laplace's equation

$$\nabla^2\Phi^{\pm} = 0. \tag{2}$$

The upper and lower boundary conditions are

$$\lim_{Z\to\infty} |\nabla\Phi^+| = 0, \tag{3}$$

$$\lim_{Z\to-\infty} |\nabla\Phi^-| = 0. \tag{4}$$

The radiation condition at $r = \infty$ is that the waves must be outgoing.

The linearized condition of continuity at the interface is

$$[\Phi_z^+]_{z=0} = [\Phi_z^-]_{z=0} = i\omega H, \tag{5}$$

where H is the elevation of the interface. From the linearized Euler equation the pressures on the upper and lower sides of the interface are

$$P^\pm = -\rho^\pm g H - [i\omega\rho^\pm \Phi^\pm]_{z=0}. \tag{6}$$

The interfacial tension T requires that

$$P^+ - P^- = \frac{T}{r}\frac{d}{dr} r \frac{\partial H}{\partial r}. \tag{7}$$

From (5), (6) and (7) the linearized interfacial boundary conditions can be expressed as

$$[\omega^2(\rho^+\Phi^+ - \rho^-\Phi^-) - g\Phi_z^+(\rho^+ - \rho^-) - (T/r)\,\partial(r\Phi_{zr}^+)/\partial r]_{z=0} = 0 \tag{8}$$

and

$$[\Phi_z^+ - \Phi_z^-] = 0. \tag{9}$$

For the region $r \geqslant R_0$, the solution to this boundary-value problem is

$$\Phi^\pm = \pm A_0 H_0^{(2)}(\kappa_0 r)\, e^{\mp\kappa_0 z} + \int_0^\infty A(\kappa)\left[\cos\kappa z - \frac{\omega^2(\rho^+ - \rho^-)}{T\kappa^3 - g\kappa(\rho^+ - \rho^-)}\sin\kappa z\right] K_0(\kappa r)\, d\kappa, \tag{10}$$

where κ_0 is defined implicitly by

$$\omega^2(\rho^+ + \rho^-) + \kappa_0 g(\rho^+ - \rho^-) - T\kappa_0^3 = 0. \tag{11}$$

$H_0^{(2)}$ is the zeroth-order Hankel function for outgoing waves. $K_0(\kappa r)$ is the zeroth-order hyperbolic Bessel function bounded for large r, and A_0 and $A(\kappa)$ are determined by the geometrical details of the oscillating rod and its amplitude of oscillation. From (5) and (10) the complex amplitude of the elevation of the interface is given by

$$H = -\frac{1}{i\omega} A_0 \kappa_0 H_0^{(2)}(\kappa_0 r) + \int_0^\infty A(\kappa)\,\kappa \frac{\omega^2(\rho^+ - \rho^-)}{T\kappa^3 - g\kappa(\rho^+ - \rho^-)} K_0(\kappa r)\, d\kappa. \tag{12}$$

A similar problem, for which the radial velocity is specified on $r = R_0$ and for which the density of the upper fluid is negligibly small, is the radial wavemaker problem which was treated by Havelock (1929), who found a solution similar to that above. A well-known result from wavemaker problems is that for $r > R_0 + \pi/\kappa_0$ the local disturbance given by the second terms of (10) and (12) is very small compared to the travelling wave disturbance given by the first term in each equation. Therefore, an accurate approximation for the elevation of the interface is

$$\begin{aligned} h_a(r,t) &= -\operatorname{Re}(1/i\omega)\,\kappa_0 A_0 H_0(\kappa_0 r)\, e^{i\omega t} \\ &= (\kappa_0/\omega)\,|A_0|[-J_0(\kappa_0 r)\sin(\omega t + \delta) - N_0(\kappa_0 r)\cos(\omega t + \delta)], \end{aligned} \tag{13}$$

where

$$\delta = \arg(A_0). \tag{14}$$

The method of determination of the interfacial tension to be used is to first find κ_0 from the results of optical measurements of the interfacial waves and then to determine the tension from (11). The basic mechanical and optical arrange-

ment considered is shown in figure 3. The general scheme is to illuminate the interface with a nearly parallel light beam and to photograph the interface. The purpose of the half-silvered mirror in the apparatus is to physically separate the camera and the light source while keeping them both on the same optical axis. For purposes of analysis, the light will be considered to be an exactly parallel beam and the axes of the light beam and the camera will be taken to be collinear as shown in figure 5. With reference to figure 5, the distance from the interface to the plane of the camera aperture is called d and the diameter of the aperture

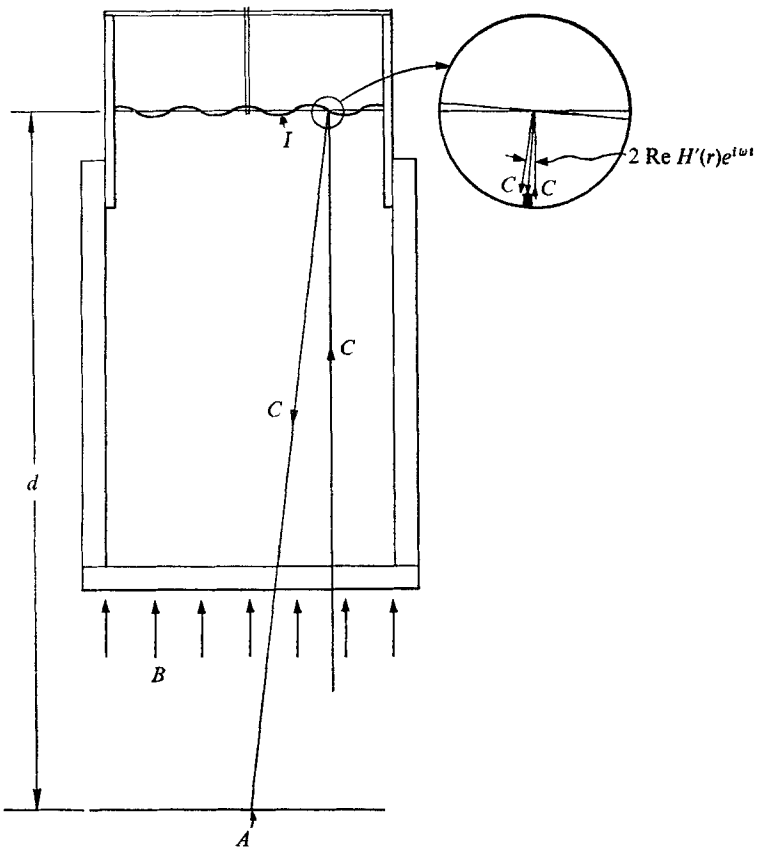

FIGURE 5. Equivalent path for a light beam C entering the camera aperture A. B is the incident light beam and I is the interface. Re $H'(r)\, e^{i\omega t}$ is the angle between the normal to the interface and the vertical z direction.

is assumed to be much smaller than d so the aperture can be considered as a point in the analysis. Geometrical optics will be used, and the angle of reflexion of the light from the interface with respect to the normal to the interface will be taken as the negative of the angle of incidence. Examination of this idealized geometry (figure 5) shows that light will be reflected into the camera from a given radius r only for one particular surface slope, as given by

$$\frac{d}{dr}\operatorname{Re} H(r)\, e^{i\omega t} = -\frac{r}{2d}. \tag{15}$$

From (12) and (15)
$$\frac{r}{2d} - \mathrm{Re}\frac{\kappa_0 A_0}{i\omega} H_1^{(2)}(\kappa_0 r)\, e^{i\omega t} = 0 \tag{16}$$

is the condition that must be satisfied for light to be reflected into the camera. A graph of the function

$$f_t(r) = \frac{r}{2d} - \mathrm{Re}\frac{\kappa_0 A_0}{i\omega} H_1^{(2)}(\kappa_0 r)\, e^{i\omega t} \tag{17}$$

for a fixed t and typical values of the various quantities is shown in figure 6. As this figure indicates, $f_t(r)$ will have only a finite number of zeros. The zeros nearest the origin occur when the second term of (17) is nearly zero and the zeros

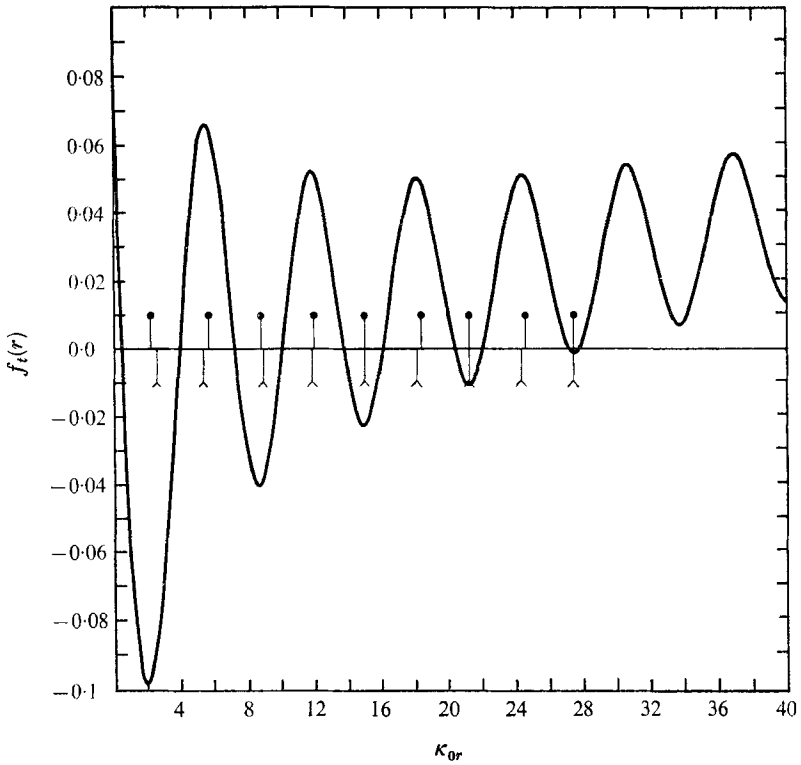

FIGURE 6. A graph of the function $f_t(r)$ as a function of $\kappa_0 r$ for $d = 185$ cm, $\kappa_0 = 5.92$ cm^{-1}, $\omega = 70$ Hz, $A_0 e^{i\omega t} = 0{\cdot}03\ (0{\cdot}995 - 0{\cdot}1i)$ cm. ●, positions midway between adjacent zero crossings of ft; ⅄, zeros in the surface elevation for the conditions of this example.

farthest from the origin occur where this term is nearly at local maximum. A photograph of the interface will show concentric bright circles at the radii for which $f_t(r)$ equals zero. The circular wave-number κ_0 is to be found from such a photograph. This cannot be done by direct comparison with (16) because A_0 is unknown.

From the characteristics of Hankel functions, it is known that there is one radius of zero surface elevation between each pair of adjacent radii of zero slope. As $\kappa_0 r$ becomes large, the radii of zero surface elevation tend to locations midway between adjacent radii of zero slope. As a result, there is one radius of zero surface elevation between adjacent zeros of $f_t(\kappa)$ if the first term of (17) is slowly

varying compared with the second term. This is the case illustrated in figure 6. Apart from the zero in surface elevation nearest the origin the zeros in the surface elevation occur for increments in $\kappa_0 r$ of very nearly π. Figure 6 shows the locations of points midway between the zeros of $f_t(\kappa)$ as well as the positions of the radii of zero surface elevation for the particular case considered. It can be seen that the spacing between zero crossings increases and decreases. Apart from the midpoints between zero crossings nearest the origin, zeros in surface elevation are better approximated by midpoints between the more closely spaced adjacent zero crossings than by the midpoints of the more widely spaced zero crossings. Therefore, the determination of κ_0 will be based on the positions of the midpoints between the more closely spaced zero crossings. If n of these midpoints are observable, excluding any midpoints very near the origin, the most accurate estimate for κ_0 is

$$\kappa_0 = 2\pi(n-1)/(r_+ - r_-), \tag{18}$$

where r_+ is the radius of the outermost midpoint used and r_- is the radius of the innermost midpoint used.

This section concludes with a discussion of the expected differences between the characteristics of the idealized model used for the preceding analysis and the expected characteristics of an experiment that would be carried out in order to measure an interfacial tension. There are three of these differences to be considered: the idealized model is for an inviscid fluid, whereas real fluids are viscous; the idealized model is for an infinite free surface, whereas an actual experiment is carried out in a cylinder of finite radius; and the idealized model has an incident light beam that is strictly parallel light, whereas an actual light beam has some angular spread.

The viscosity of actual fluids results in a viscous attenuation of the wave amplitude with increasing radius. Examination of figure 6 shows that this will cause negligible error in the measurement of κ_0 if the attenuation is small over the distance between adjacent zero crossings of $f_t(r)$ used for estimation of the positions of zero surface elevation. An approximate calculation of the viscous damping of small amplitude two-dimensional gravity waves in a fluid of density ρ and viscosity μ has been carried out by Milne-Thomson (1960, pp. 580–1). The basis of the approximation is that fluid motion retains its irrotational character during the damping process. The result is that the wave amplitude h_t behaves as

$$h_t = h_0 \exp[-2\kappa_0^2 t\mu/\rho], \tag{19}$$

where h_0 is the amplitude of the wave at $t = 0$. This formula gives the rate of amplitude decay observed while following a single point on the surface moving at the phase velocity of the wave. When an analysis similar to Milne-Thomson's is carried out for axisymmetric cylindrical waves under the influence of both gravity and surface tension, the identical result is obtained. For waves on the interface of two fluids the result is very similar,

$$h_a = h_0 \exp[-2\kappa_0^2 t(\mu^+ + \mu^-)/(\rho^+ + \rho^-)]. \tag{20}$$

The error due to the viscous attenuation is related to the decay in wave amplitude between adjacent zero crossings of $f_t(r)$. Use of midpoints between the more closely spaced zero crossings results in less error from viscous attenuation than

would result from use of midpoints between more widely spaced zero crossings. The distances between the closer pairs of zero crossings are typically about one-quarter of a wavelength. When the gravity effects are negligible compared to interfacial tension effects, equations (11) and (20) give the attenuation over a one-quarter wavelength $\frac{1}{4}\lambda$ as

$$\frac{h_a(r+\frac{1}{4}\lambda)}{h_a(r)} = \exp\{-\pi\kappa_0^{-\frac{1}{2}}[\mu^+ + \mu^-]/[T(\rho^+ + \rho^-)]^{\frac{1}{2}}\}. \tag{21}$$

This indicates that for given fluids κ_0 should be made as large as possible, consistent with other constraints of the experiment.

The difference between carrying out the experiment in a vessel of finite radius and the model having an infinite radius is that the wall of the vessel reflects the wave incident upon it. In the presence of outgoing and incoming waves, (13) would take the form

$$h_a(r_1 t) = -\mathrm{Re}\,(1/i\omega)\, e^{i\omega t}[A_0 H_0^{(2)}(\kappa_0 r) + B_0 H_0^{(1)}(\kappa_0 r)], \tag{22}$$

where A_0 and B_0 are constants. For non-zero values of B_0 the subsequent analysis would remain entirely unchanged from the preceding analysis apart from introduction of the two complimentary Hankel functions, and no errors would be introduced.

The effect of having a beam of light with some angular spread is to make the bright rings that would appear in a photograph using parallel light take the form of bright bands. If the distribution of light intensity were highest in the direction of normal incidence on the plane of the undisturbed interface, and the brightest part of the bands in a photograph were taken as the zero crossings of $f_t(r)$, no error would be introduced. However, in actual use the exact position of the brightest part of the bands cannot be determined so that some error is introduced by the angular spread of the light beam.

3. Experiments

An experimental apparatus embodying the concepts shown in figure 3 was constructed for purposes of measuring interfacial tensions. The cylindrical vessel containing the interface had a diameter of 4·5 cm and illumination was provided by a stroboscopic flash lamp mounted in a parabolic reflector. The duration of the flash was about one microsecond. The camera was adjusted to give an image magnification of 2:1, d was 11·43 cm and the camera aperture diameter was 0·17 cm.

In order to test the apparatus and method, initial tests were carried out on an air–tap-water interface. The density of the tap water was 1·0 g/cm^3. The surface tension of this interface was measured by the capillary tube method as 64 dynes cm. Figure 7 (plate 1) shows photographs of the interface made with the apparatus for oscillation frequencies of 80 Hz. Examination of (11) shows that for the conditions of this experiment the ratios of the second term to the first term, and the second term to the third term are very much smaller than unity. Therefore, the second term can be neglected yielding

$$T = (2\pi)^2 f^2(\rho^+ + \rho^-)/K_0^3, \tag{23}$$

where
$$f = \omega/2\pi. \tag{24}$$

Since the wavelength λ is directly measured where

$$\lambda = \kappa_0/2\pi, \tag{25}$$

a more convenient form of (23) is

$$T = f^2(\rho^+ + \rho^-)\lambda^3/2\pi. \tag{26}$$

In order to determine the most accurate estimate of λ, the distance corresponding to as many wavelengths as are accurately observable is measured on a photograph, and this distance is divided by the number of integer wavelengths to obtain λ. Values of λ as measured from the photographs of figure 6 are $0{\cdot}395 \pm 0{\cdot}010$ cm for the 80 Hz case and $0{\cdot}305 \pm 0{\cdot}005$ cm for the 120 Hz case.

Using (26) gives $T = 63{\cdot}0 \pm 5{\cdot}0$ dynes/cm for the former case and $T = 65{\cdot}3 \pm 3{\cdot}5$ dynes/cm for the later case. These values agree with each other and with the value of the surface tension measured by the capillary tube method within the limits of the error in the measurement of λ from the photographs.

Figure 8 (plate 2) shows photographs of a water–oil interface for oscillation frequencies of 20 Hz and 100 Hz. The water was tap water and the oil was South Louisiana Crude. The density of the tap water was $1{\cdot}0$ g/cm^3 and the density of the oil was $0{\cdot}84$ g/cm^3. The measured wavelengths are $0{\cdot}345 \pm 0{\cdot}010$ cm for the 30 Hz case and $0{\cdot}153 \pm 0{\cdot}005$ cm for the 100 Hz case yielding values of the interfacial tension of $10{\cdot}8 \pm 1{\cdot}0$ dynes/cm for the former case and $10{\cdot}8 \pm 0{\cdot}8$ dynes/cm for the latter.

4. Discussion

Two features of the photographs of the water–oil interface (figure 8) are in need of explanation. The first is the outermost bright ring which has nothing to do with the waves. This ring results from the angle of the meniscus at the ring being that value that reflects light into the camera. The wall of the vessel is visible near the corners of the photographs indicating that the radial extent of the meniscus is unusually large. This is due to the relatively small value of the density difference between the oil and water and the relatively small surface tension. The second feature is the appearance of the secondary visible bands in figure 8(*b*). The third pair of bright bands corresponds to the outermost pair that should be visible according to the theory of § 2. The reasons for the visibility of the secondary bands, which are less bright than the primary bands, are not known for certain at this time, but it is thought that they are related to the angular spread of the incident light beam.

The experimental results of § 3 indicate that the theory for measuring liquid–liquid interfacial tensions presented in § 2 is sufficiently accurate for use in the measurement of such tensions. The primary inaccuracy in such measurements is that related to the measurement of the wavelength λ. Equation (23) shows that the surface tension is proportional to λ^3 so that small fractional errors in the measurement of λ lead to substantially larger fractional errors in the resulting estimate of the interfacial tension. For this reason it is important to minimize

errors in the measurement of λ when applying the technique given here for the determination of interfacial tensions.

This work was supported in part by the U.S. Coast Guard under contract number DOT-CG-01-381A.

REFERENCES

BARTELL, F. E. & MILLER, F. L. 1928 A method for the measurement of the interfacial tension of liquid–liquid systems. *J. Am. Chem. Soc.* **50**, 1961–1967.

FAY, J. A. 1969 The spread of oil slicks on a calm sea. *M.I.T. Fluid Mechanics Lab Rep.* no. 69–6.

HAVELOCK, T. H. 1929 Forced surface-waves on water. *Phil. Mag.* S7, **8**, 569–576.

MILNE-THOMSON, L. M. 1960 *Theoretical Hydrodynamics.* Macmillan.

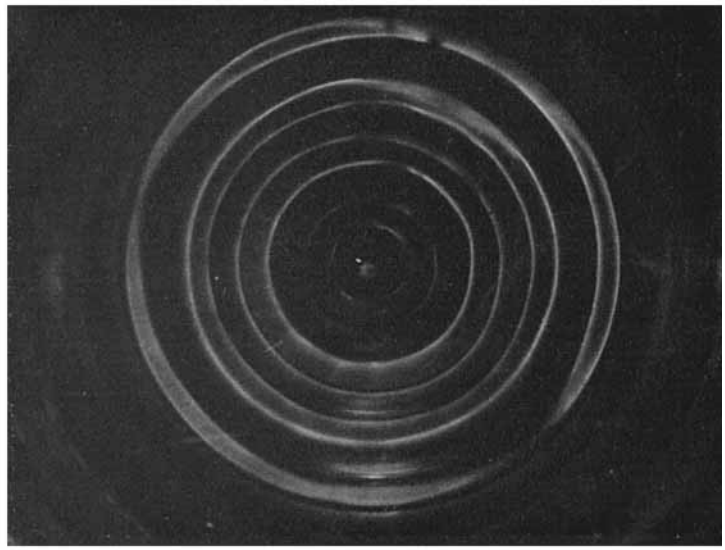

(*a*)

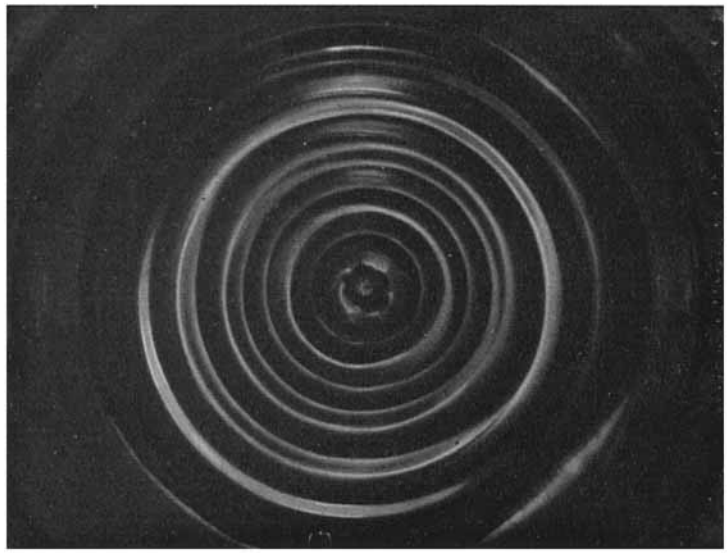

(*b*)

FIGURE 7. Photographs of waves on a water–air interface with a magnification factor of two. (*a*) $f = 80$ Hz, (*b*) $f = 120$ Hz.

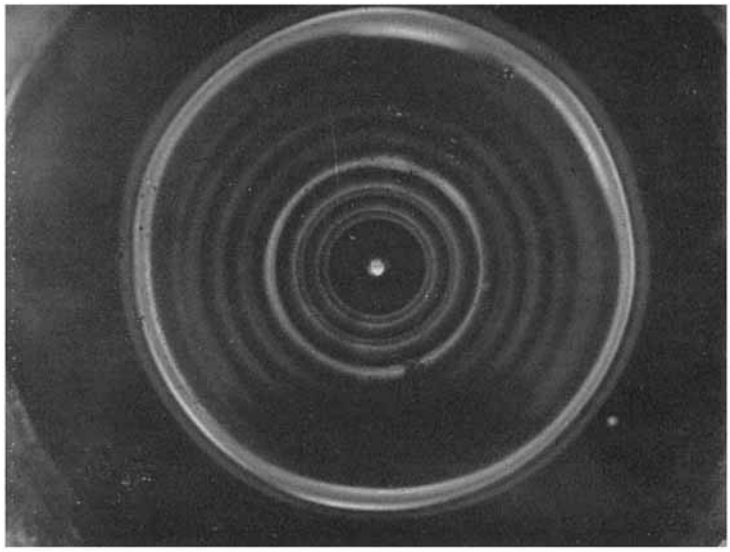

(*a*)

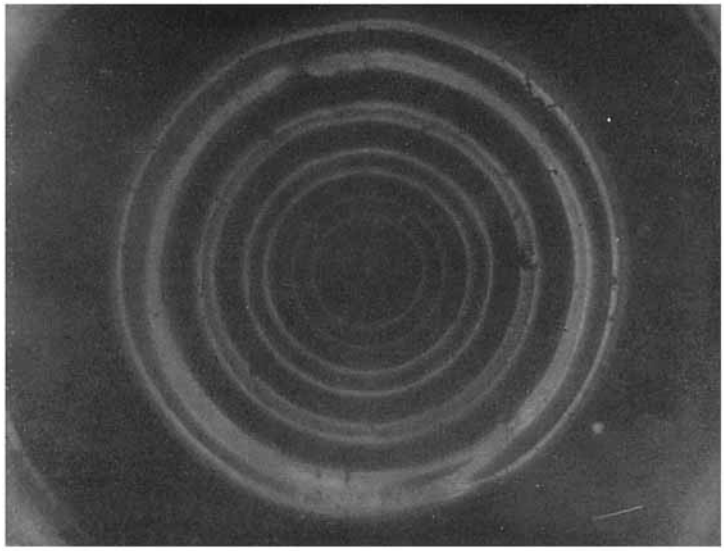

(*b*)

FIGURE 8. Photographs of waves on an oil–water interface with a magnification factor of two. (*a*) $f = 30$ Hz, (*b*) $f = 100$ Hz.